

## Review

## Temperature effect and thermal impact in lithium-ion batteries: A review

Shuai Ma<sup>a,1</sup>, Modi Jiang<sup>a,1</sup>, Peng Tao<sup>a</sup>, Chengyi Song<sup>a</sup>, Jianbo Wu<sup>a</sup>, Jun Wang<sup>b,\*</sup>, Tao Deng<sup>a,\*</sup>, Wen Shang<sup>a,\*</sup>

<sup>a</sup> School of Materials Science and Engineering, and State Key Laboratory of Metal Matrix Composites, Shanghai Jiao Tong University, 800 Dongchuan Rd, Shanghai 200240, PR China

<sup>b</sup> A123 Systems Research Center, 200 West Street, Waltham, MA 02451, USA



## ARTICLE INFO

## Keywords:

Lithium-ion battery  
Temperature effect  
Internal temperature  
Battery management  
Thermal management

## ABSTRACT

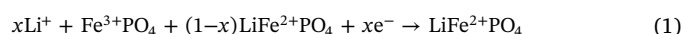
Lithium-ion batteries, with high energy density (up to 705 Wh/L) and power density (up to 10,000 W/L), exhibit high capacity and great working performance. As rechargeable batteries, lithium-ion batteries serve as power sources in various application systems. Temperature, as a critical factor, significantly impacts on the performance of lithium-ion batteries and also limits the application of lithium-ion batteries. Moreover, different temperature conditions result in different adverse effects. Accurate measurement of temperature inside lithium-ion batteries and understanding the temperature effects are important for the proper battery management. In this review, we discuss the effects of temperature to lithium-ion batteries at both low and high temperature ranges. The current approaches in monitoring the internal temperature of lithium-ion batteries via both contact and contactless processes are also discussed in the review.

## 1. Introduction

Electrochemical batteries, first invented by Alessandro Volta in 1800 [1–4], have become one of the necessities in human's life. Electrochemical batteries can be classified into primary batteries and secondary batteries [5–7]. Primary batteries are used only once and cannot be recharged, which is due to the irreversible electrochemical reactions occurring in the batteries. Zinc–carbon batteries are one of the representative primary batteries [8,9]. On the contrary, secondary batteries, which are also called rechargeable batteries, are electrochemical batteries that can be cyclically reused by discharging and recharging. Such reusable function originates from the reversible electrochemical reactions that occur in the batteries. Although primary batteries hold the major part of the commercial battery market, there are challenges associated with the use of primary batteries, including the generation of large amounts of unrecyclable materials, and the toxic components in the batteries that post environmental concerns [10–12]. The development of secondary batteries rises rapidly, including the development of nickel–metal hydride batteries [13–15], lithium-ion batteries (LIBs) [16–18], and sodium-ion batteries [19–21]. Among these secondary batteries, LIBs, which exhibit high energy density and excellent working performance [22–25], are leading the current secondary

battery market and widely used in many different areas.

The first commercial LIB, introduced by Sony Corporation in 1991 [26,27], led a revolution of the battery market. A common LIB consists of lithium compound-based cathode, carbon-based anode, electrolyte and separator. In general, the cathode materials are coated on an aluminum foil and the anode materials are coated on a copper foil, respectively. The aluminum and copper serve as the current collectors. A piece of porous polymer separator that is immersed in electrolyte and sandwiched between the anode and cathode prevents the shorting of the two electrodes (Fig. 1A). As shown in Fig. 1B, lithium ions go through the cycles of intercalation and deintercalation, and shuttle through the electrolyte as charge carriers in the internal circuit. With the intercalation and deintercalation of lithium ions, redox reactions occur at the electrodes, which generate electrons that move directionally through the external circuit to form the current. The following equations show the redox reactions occurring at LiFePO<sub>4</sub> cathodes (Eq. (1)) and carbon anodes (Eq. (2)) during discharging.



The migration of lithium ions in internal circuit and electrons in external circuit leads to the operation of LIBs. The operation rate,

Peer review under responsibility of Chinese Materials Research Society.

\* Corresponding authors.

E-mail addresses: [junwang@123systems.com](mailto:junwang@123systems.com) (J. Wang), [dengtao@sjtu.edu.cn](mailto:dengtao@sjtu.edu.cn) (T. Deng), [shangwen@sjtu.edu.cn](mailto:shangwen@sjtu.edu.cn) (W. Shang).

<sup>1</sup> These authors contributed equally.

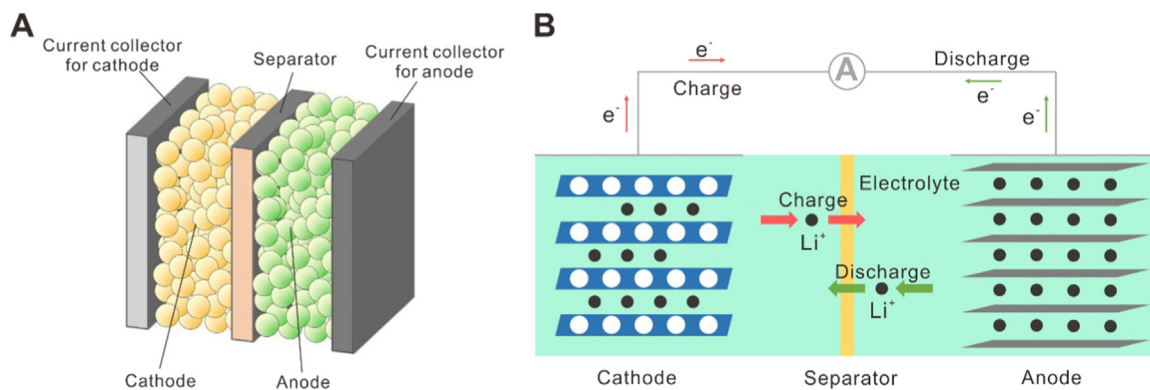


**Fig. 1.** (A) Schematic of the components and structures of LIBs. Reproduced with permission from [39]. Copyright: 2017, Elsevier. (B) Schematic of the operating mechanism of LIBs. Reproduced with permission from [40]. Copyright: 2017, Wiley-VCH.

known as charging or discharging rate, is referred as C rate, which is defined as the charging or discharging current divided by the capacity of LIBs.

Due to the high energy density (up to 705 Wh/L [28]) and power density (up to 10,000 W/L [29]), high voltage capability [30] and great cycling performance [31], LIBs are used as power sources in numerous electronic products [32,33], electric vehicles [25,34], energy storage systems [35,36] as well as in military and aerospace applications [37,38].

The LIBs, however, are still facing barriers that limit their application space [18,41]. One of the major limitations is the impact of temperature to the proper operation of the LIBs. Generally, the acceptable temperature region for LIBs is  $-20\text{ }^\circ\text{C} \sim 60\text{ }^\circ\text{C}$  [42]. Pesaran et al. [43] showed that the optimal temperature range for LIBs is  $15\text{ }^\circ\text{C}\text{--}35\text{ }^\circ\text{C}$ . Once the temperature is out of these comfortable regions, LIBs will degrade fast with increased risk of facing safety problems that include fire and explosion. In general, impacts from temperature can be divided into two categories: low temperature effects and high temperature effects [44–47].

Low temperature effects mostly take place in high-latitude country areas, such as Russia, Canada and Greenland Island [48,49]. In these areas, the outdoor temperatures in winter are much lower than  $0\text{ }^\circ\text{C}$ . Such low temperatures will affect the performance and life of LIBs, especially for those used in pure electric vehicles (EVs), hybrid electric vehicles (HEVs), and plug-in hybrid electric vehicles (PHEVs) [48,50]. Another cold environment that involves the use of LIBs is the outer space. For example, the temperature on Mars [51] can be as low as  $-120\text{ }^\circ\text{C}$ , which poses serious challenge to the use of LIBs in astro-vehicles for space exploration. At these low operating temperatures, LIBs will show slow chemical-reaction activity and charge-transfer velocity [42], which leads to the decrease of ionic conductivity in the electrolytes [52] and lithium-ion diffusivity within the electrodes [53]. Such decrease will result in the reduction of energy and power capability, and sometimes even performance failure.

Compared to the low temperature effects that are mostly limited to the low temperature application environments, the high temperature effects happen in a much broad range of application environments, including not only high temperature environments but also low temperature environments. The environmental temperature plays a critical role in low temperature effects, while most of time high temperature effects are attributed to the high internal temperature of LIBs during operation rather than the environmental temperature. The high internal temperature is caused by heat generation inside the LIBs, which happens at high current state, including operations with fast charging rate and fast discharging rate [54,55]. The high temperature effects will also lead to the performance degradation of the batteries, including the loss of capacity and power [56–59]. Generally, the loss of lithium and the reduction of active materials under high temperature will result in the

loss of the capacity [60], while the increase of internal resistance is responsible for the loss of power [61]. If the temperature is out of control, thermal runaway will be triggered, which may lead to self-ignition and even explosion in some cases [62,63].

Proper management of the operating temperature of LIBs is thus critical to the performance and safe operation of the batteries. Accurate temperature monitoring of LIBs is one of the important processes in proper temperature management. It is, however, difficult to monitor the temperature distribution inside the batteries, which are tightly sealed during operation. In this review, we will overview both the adverse effects of temperature to LIBs, and the different approaches in monitoring internal temperature of LIBs.

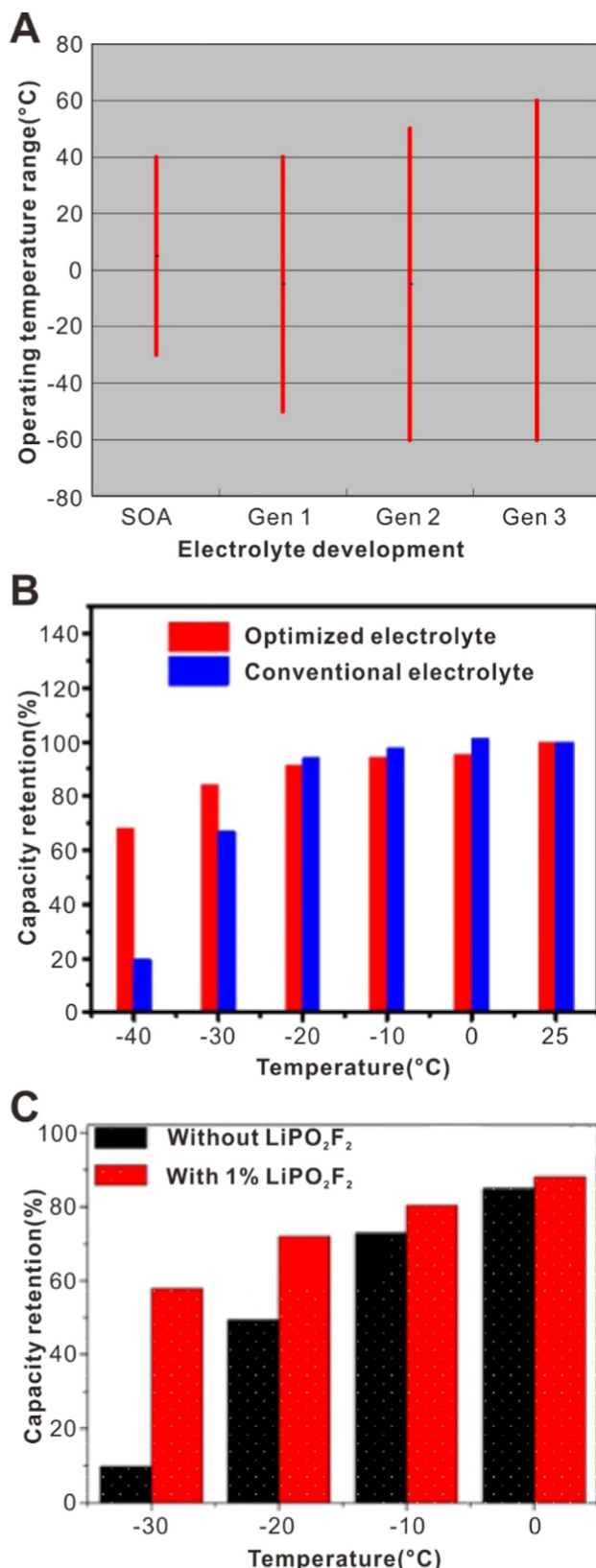
## 2. The effects of temperature to LIBs

Most of the temperature effects are related to chemical reactions occurring in the batteries and also materials used in the batteries. Regarding chemical reactions, the relationship between the rate of chemical reactions and reaction temperature follows Arrhenius equation, and temperature variation can lead to the change of electrochemical reaction rate in batteries [64]. Besides chemical reactions, the ionic conductivities of electrodes and electrolytes are also affected by temperature. For example, the ionic conductivity of lithium salt based electrolytes decreases at low temperatures [65]. With these effects in concern, the LIBs used in EVs and HEVs can hardly meet the expectation of a 10-year life suggested by the United States Advanced Battery Consortium (USABC) [66]. In the following sections we will discuss both the low temperature effects and the high temperature effects on the LIBs.

### 2.1. Low temperature effects

The performance of LIBs will degrade at temperatures below  $0\text{ }^\circ\text{C}$  [48,67]. In 2001, Nagasubramanian showed that the power and energy densities of Panasonic 18650 LIBs were  $\sim 800\text{ W/L}$  and  $\sim 100\text{ Wh/L}$  at  $25\text{ }^\circ\text{C}$ , and these values were reduced by 98.75% and 95% to  $< 10\text{ W/L}$  and  $\sim 5\text{ Wh/L}$  at  $-40\text{ }^\circ\text{C}$  [68]. In another report, the state of charge (SOC) of a LIB, which is defined as the ratio of the present residual capacity to the overall available capacity [69], was also found to decrease by  $\sim 23\%$  when the operating temperature decreased from  $25\text{ }^\circ\text{C}$  to  $-15\text{ }^\circ\text{C}$  [70].

With the complex material system used in LIBs, the performance degradation at low temperatures can be attributed to several different sources. First, the low temperature will affect the property of electrolyte. With the decrease of temperature, the viscosity of the electrolyte will increase, which will reduce the ionic conductivity. The internal resistance will subsequently rise due to the increase in the impedance of the directional migration of chemical ions. To counter such effect,



electrolytes with low freezing point were explored, and different electrolyte additives were studied [51,71–74]. Bugga et al. [51] presented a guideline for developing formulations of low temperature electrolytes during their research of LIBs for space applications. The improved

**Fig. 2.** Researches on electrolytes for improving the performance of LIBs at low temperatures. (A) Comparison of the operating temperature range between three generations of electrolytes (Gen 1, Gen 2 and Gen 3) of Exploration Systems Missions Directorate (ESMD) programs and the state of art (SOA) operating temperature range. Reproduced with permission from [51]. Copyright: 2007, IEEE. (B) Comparison of the capacity retention at different temperatures between the optimized electrolyte and conventional electrolyte. Reproduced with permission from [75]. Copyright: 2017, American Chemical Society. (C) The effect of using LiPO<sub>2</sub>F<sub>2</sub> as the additive to the electrolyte on the capacity retention at different temperatures. Reproduced with permission from [74]. Copyright: 2008, Elsevier.

electrolytes can be used in an extended operating temperature range (Fig. 2A) and were proved to be effective in aerospace batteries. Li et al. [75] also reported an optimized electrolyte formulation of 1.0 M LiPF<sub>6</sub> in ethylene carbonate(EC) – propylene carbonate(PC) – ethyl methyl carbonate (EMC) (1:1:8 by wt) with 0.05 M CsPF<sub>6</sub>. Such formulation enabled a capacity retention of 68% for the batteries tested at -40 °C, while the ones with conventional formulation only showed a capacity retention of 20% (Fig. 2B). Specific electrolyte additives, such as lithium difluorophosphate (LiPO<sub>2</sub>F<sub>2</sub>), were also proved to be effective in improving the performance of LIBs at low temperature (Fig. 2C) [74].

The increase of charge-transfer resistance in LIBs is also an important factor that contributes to the performance degradation at low temperatures. The charge-transfer resistance of LiFePO<sub>4</sub>-based cathodes at -20 °C was reported to be three times higher than that at room temperature [76]. Such high charge-transfer resistance largely affects the kinetics in batteries. The study of LIB performance at low temperatures by Zhang et al. [77] demonstrated that the charge-transfer resistance significantly increased when the temperature decreased. The charge-transfer resistance of a discharged battery normally is much higher than that of a charged one. Charging a battery at low temperatures is thus more difficult than discharging it. Additionally, performance degradation at low temperatures is also associated with the slow diffusion of lithium ions within electrodes. Such slow down can be countered by altering the electrode materials with low activation energy. For example, Li<sub>3</sub>V<sub>2</sub>(PO<sub>4</sub>)<sub>3</sub> (LVP), which has an activation energy of 6.57 kJ mol<sup>-1</sup>, showed a 200x improvement of apparent chemical diffusion coefficient of lithium ions over LiFePO<sub>4</sub> (LFP) with an activation energy of 47.48 kJ mol<sup>-1</sup> at -20 °C [78].

Another typical effect that occurs at low temperatures is lithium plating [79–81]. The cold condition will trigger the polarization of anodes and lead to the approach of the potential of graphite and other carbon based anodes to that of lithium metal, which would slow down the lithium-ion intercalation into the anodes during charging process [82]. The aggregated lithium ions are thus deposited on the surface of the electrodes, which causes the reduction of the battery capacities. Furthermore, the lithium plating exists in the form of dendrite, which may penetrate the separators, and result in the internal short-circuit [83].

## 2.2. High temperature effects

The effects at high temperatures are much more complex than those at low temperatures. During the operation of the LIBs, heat is generated inside the batteries, and understanding the heat generation is critical in minimizing the high temperature effects in LIBs.

### 2.2.1. Heat generation

In general, the heat generation within the LIBs at normal temperature is associated with charge transfer and chemical reactions during charging and discharging [84,85]. The heat is generated either in the reversible process or the irreversible process in LIBs [84,86–88]. Fig. 3 shows the possible heat generation within LIBs. The heat generated in the reversible process, also known as entropic heat, originates from the reversible entropy change during electrochemical reactions [89]. There

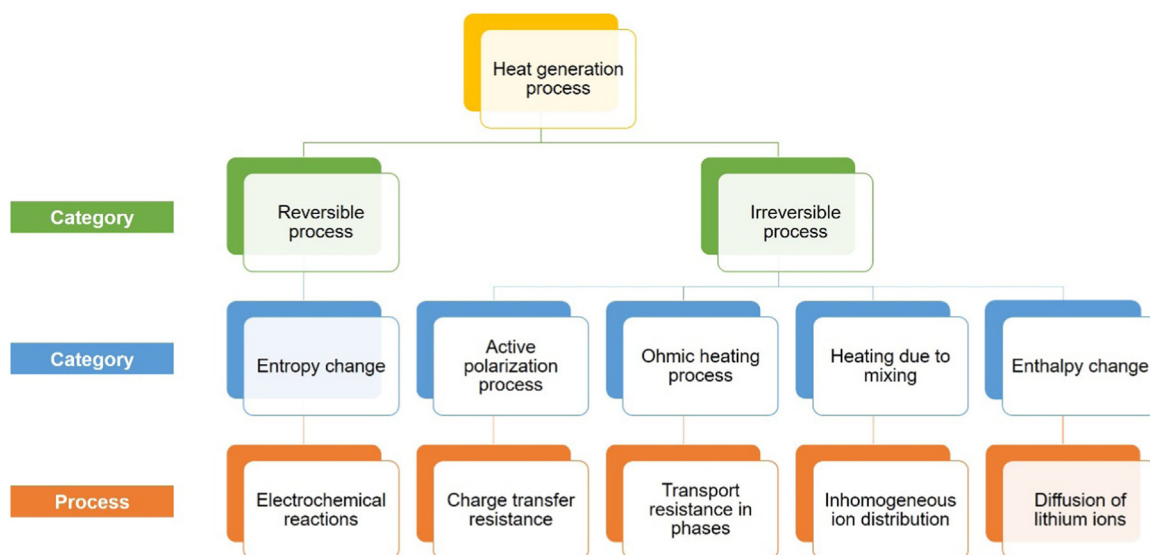


**Fig. 3.** Illustration of categories and process of the heat generation within LIBs.

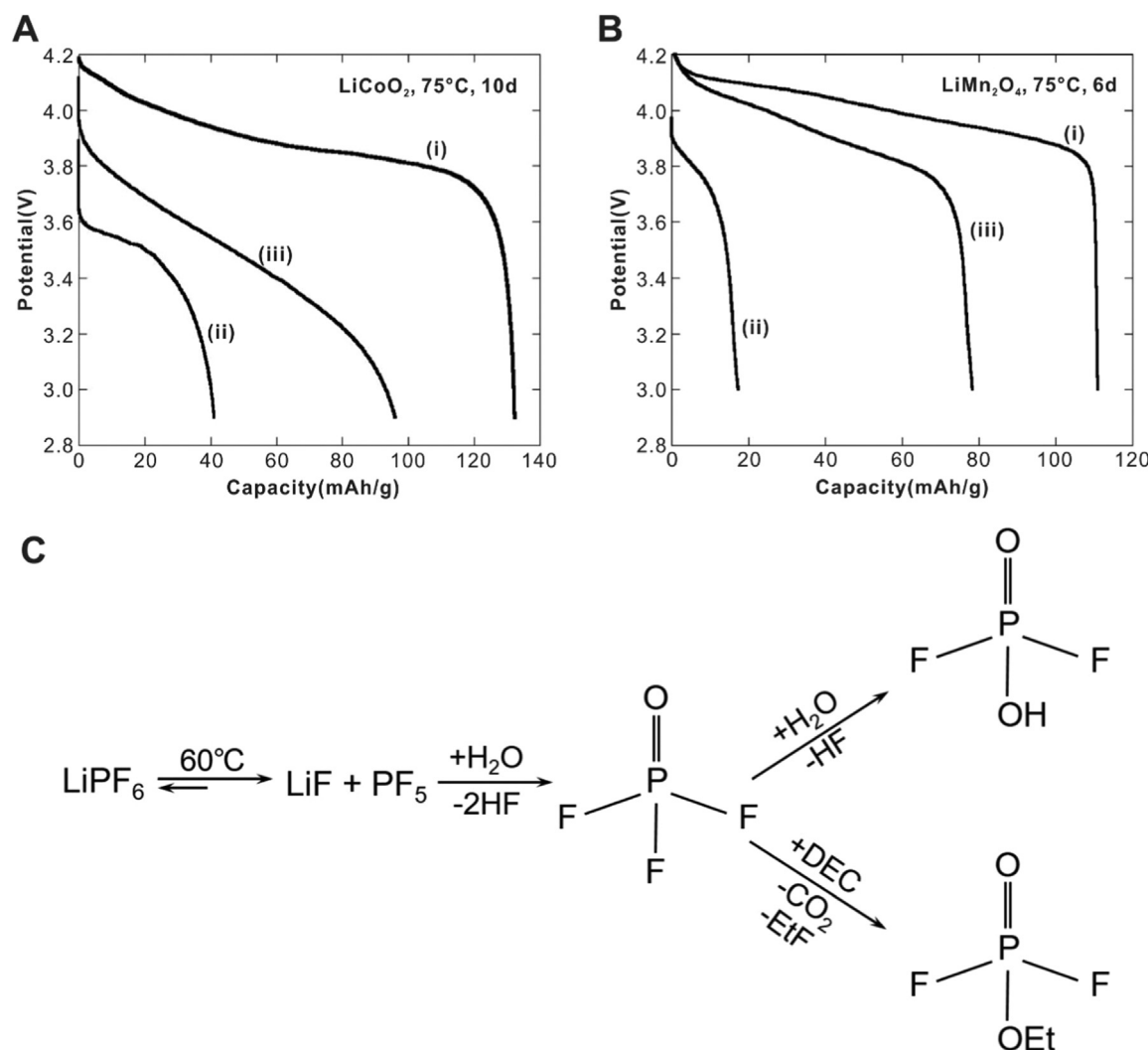


**Fig. 4.** Discharge curves of batteries with (A) $\text{LiCoO}_2$  and (B) $\text{LiMn}_2\text{O}_4$  cathodes before and after aging at  $75^\circ\text{C}$  for 10 days and 6 days, respectively, (i) after the 5th cycle before aging, (ii) after the 1st cycle after aging, (iii) after the 5th cycle after aging. Reproduced with permission from [101]. Copyright: 2006, Elsevier. (C) Schematic of the decomposition pathway of  $\text{LiPF}_6$  with proton impurities at  $60^\circ\text{C}$ . Reproduced with permission from [104]. Copyright: 2014, Elsevier.

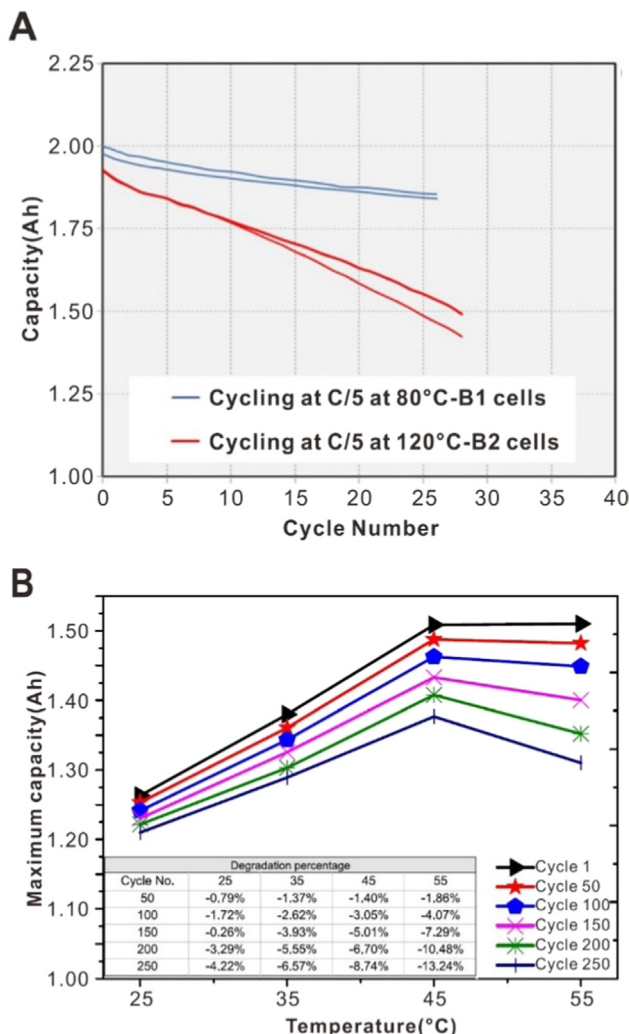


**Fig. 5.** (A) Capacity change with cycle number of batteries cycling at C/5 rate at 85 °C and 120 °C, respectively. B1 cells: After two initial cycles at 60 °C, the cells were cycled at 85 °C between 2.7 V and 4.1 V for 15 days; B2 cells: After two initial cycles at 60 °C, the cells were cycled at 120 °C between 2.7 V and 4.1 V for 15 days. Reproduced with permission from [102]. Copyright: 2013, Elsevier. (B) Maximum capacity change and degradation percentage of the tested LIB with temperature after various cycle numbers. Reproduced with permission from [105]. Copyright: 2015, Springer Nature Limited.

are many possible irreversible processes that can generate heat, including active polarization process, ohmic heating process, heating due to mixing and enthalpy change [90–92]. The polarization is resulted from the overpotential between operating potential and open circuit potential of the batteries. It leads to the increase of charge transfer resistance at electrode-electrolyte interface, or Solid Electrolyte Interface (SEI). When lithium ions overcome such resistance at interface for their intercalation/deintercalation, heat is produced [93]. The ohmic heating process occurs in both the electrode and electrolyte. It is due to the resistance of electrodes and electrolytes that hinders the transportation of charges [85,94]. When the LIBs are in operation, either in charging or in discharging, the ion distribution becomes inhomogeneous, which can lead to the mixing of ions and the generation of heat during mixing [84,95]. Another form of irreversible process that generates heat is the enthalpy change due to phase change in cathodes, which is primarily due to the diffusion of lithium ions [96].

### 2.2.2. Aging

Aging is an effect during the application of LIBs at high

temperatures. Aging not only affects the performance of LIBs, but also reduces their lifetime. In general, the aging of LIBs includes cycle aging and calendar aging [97,98]. These two types of aging, however, always occur in combination due to the complex composition and working process of LIBs [99]. Increasing the operating temperature of LIBs above the optimal scope will accelerate the aging process and lead to the degradation of LIBs. Most of research in this area focuses on aging of either the individual components inside the battery [100,101] or the battery system [102,103].

For the thermal aging effects on individual components, the studies mostly center on electrodes and electrolytes. Gabrisch et al. [101] studied the capacity change of LiCoO<sub>2</sub> and LiMn<sub>2</sub>O<sub>4</sub> cathodes. The LiCoO<sub>2</sub> and LiMn<sub>2</sub>O<sub>4</sub> cathodes went through thermal aging at 75 °C for 10 days and 6 days, respectively. The discharge profiles of these two cathodes showed the severe loss of capacity after aging treatment (Fig. 4A and B). The authors indicated that the thermal-induced crystallographic transformation led to an irreversible intercalation of lithium ions into cathode lattices, which resulted in the loss of capacity of the cathodes. Handle et al. [104] studied the decomposition of lithium hexafluorophosphate (LiPF<sub>6</sub>), which is a commonly used conductive salt in electrolytes, under thermal aging. With the existence of proton impurities, the decomposition of LiPF<sub>6</sub> is enhanced at high temperature. Fig. 4C shows the decomposition pathway of LiPF<sub>6</sub> in a mixture of ethylene carbonate (EC) and diethylene carbonate (DEC) (1:2, v-v) at 60 °C, which led to the formation of difluorophosphoric acid as the main decomposition product.

Compared to the studies of individual components, studies of the entire battery system provide a more comprehensive demonstration of high temperature aging effects of LIBs. Bodenes et al. [102] studied the aging process of Li(Ni, Mn, Co)O<sub>2</sub> (NMC)-based LIBs. Fig. 5A shows that the loss of capacity of the tested battery was 7.5% when it was cycled at 85 °C, while it reached to 22% when cycled at 120 °C. By characterizing the change of binder and SEI during aging process with various characterization methods, they provided two possible reasons for the aging degradation. On one hand, the polyvinylidene fluoride (PVDF) binder migrated to the surface of anodes and impeded the intercalation of lithium ions. On the other hand, the carbonates species disappeared and inorganic species increased at the SEI layers at high temperature, which led to the increase of impedance inside the batteries. Based on the electrochemistry-based electrical (ECBE) model, Leng et al. [105] investigated the temperature effect on the rate of capacity degradation of a Sony Prismatic LIB during aging from 25 °C to 55 °C (Fig. 5B). As shown in Fig. 5B, elevating temperature in the tested range partially increased the capacity of battery, but it also accelerated the rate of degradation of capacity during cycling. The increase of degradation rate was mainly ascribed to the degradation of electrodes, where the phase change and surface modification were aggravated at high temperatures.

### 2.2.3. Thermal runaway

Thermal runaway may happen when the batteries are manufactured defectively or handled improperly. Thermal runaway often occurs at high temperature states, in which the high temperature triggers the exothermic reactions in the operating batteries [63]. These reactions release more heat, and in turn further promote the increase of temperature within the batteries [106]. When such uncontrolled heat generation exceeds the heat endurance of the batteries, fire and explosion would occur [63]. Many notebook manufacturers such as Apple and Lenovo recalled their products and suffered huge financial losses in the past decades due to thermal runaway issues [107,108]. Hence, understanding the thermal runaway of LIBs is important to the thermal management of batteries at high temperatures.

Finegan et al. [109] first introduced the technology of *in-operando* high-speed synchrotron X-ray computed tomography and radiography into the diagnosis of thermal runaway behaviors of commercial 18650 LIBs (Fig. 6A). With the simulation of the thermal condition using a heat gun, thermal runaway occurred when the temperature of battery

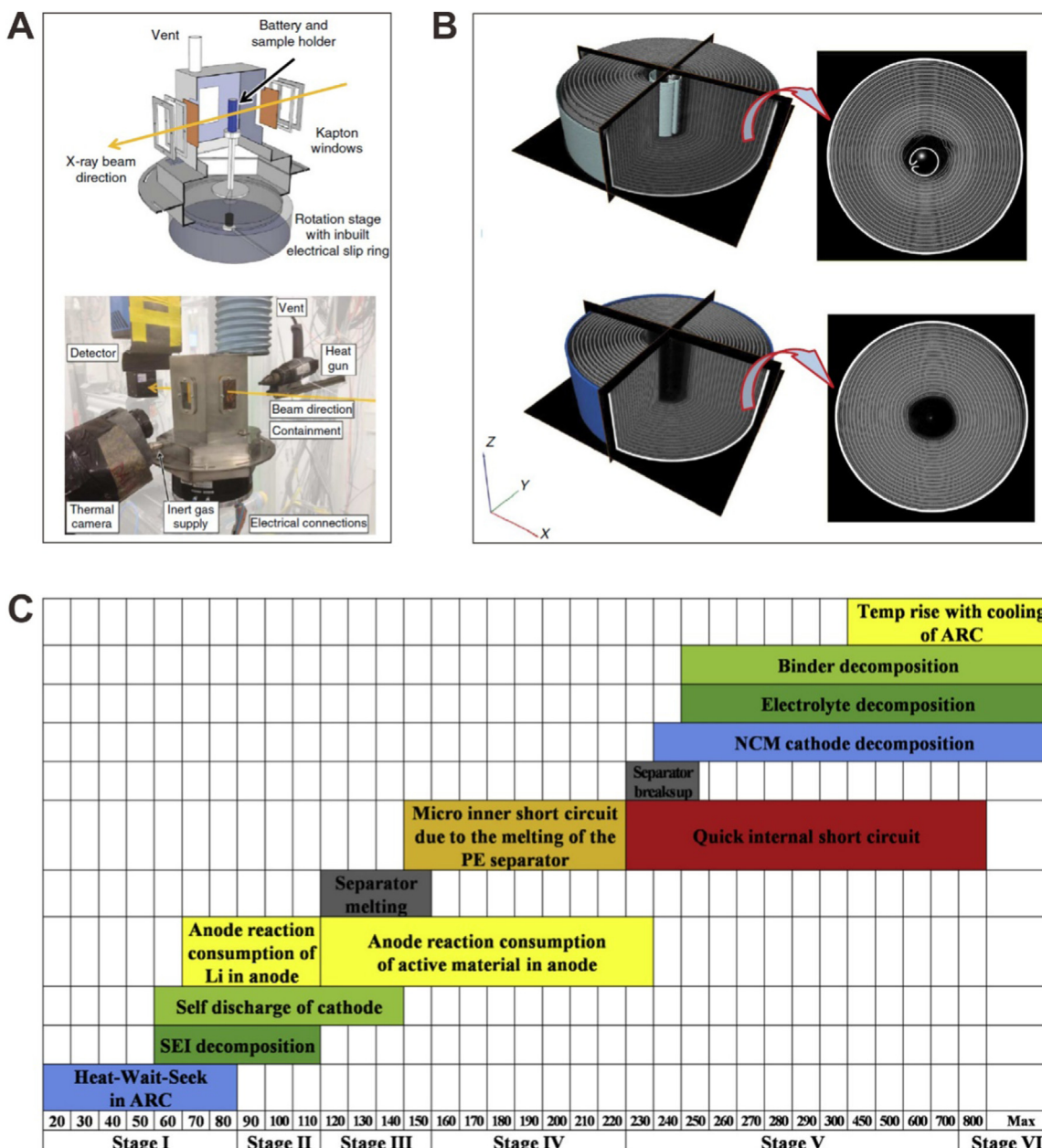


**Fig. 6.** (A) Schematic of the in-operando experimental setup. (B) 3D reconstruction and the cutoff top view of the tested cylindrical batteries. (A,B) Reproduced with permission from [109]. Copyright: 2015, Springer Nature Limited. (C) Thermal runaway stages described at different temperature ranges. Reproduced with permission from [110]. Copyright: 2014, Elsevier.

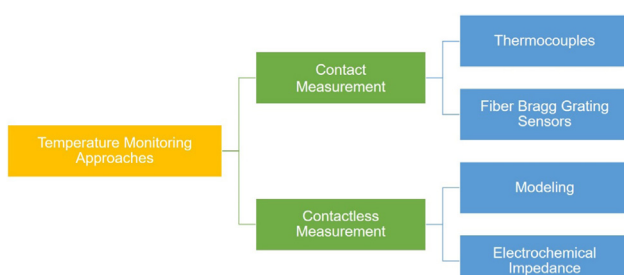


**Fig. 7.** Classification of current approaches for monitoring the internal temperature of LIBs.

shell exceeded 200 °C. With the propagation of thermal runaway, the electrodes decomposed and gas flew through the vent continuously, resulting in the collapse of internal structures. In the later period of thermal runaway, the copper foil also melted and turned into globules. This phenomenon indicated that the local internal temperature even exceeded 1000 °C, since the melting point of copper is 1085 °C. This work provided a novel approach in studying the thermal failure mechanism of LIBs.

In addition to the damage of materials and structures in the batteries, many studies also focus on the process of thermal runaway [50,110]. Fig. 6B provides an example of thermal runaway process propagating with the increase of temperature [110]. In stage I, the loss of capacity occurs at elevated temperature. The decomposition of SEI happens after the temperature reaches 60 °C (stage II). Without the covering of SEI layers, the anodes directly contact with the electrolytes and react with them at 100 °C. This reaction is an exothermic reaction,

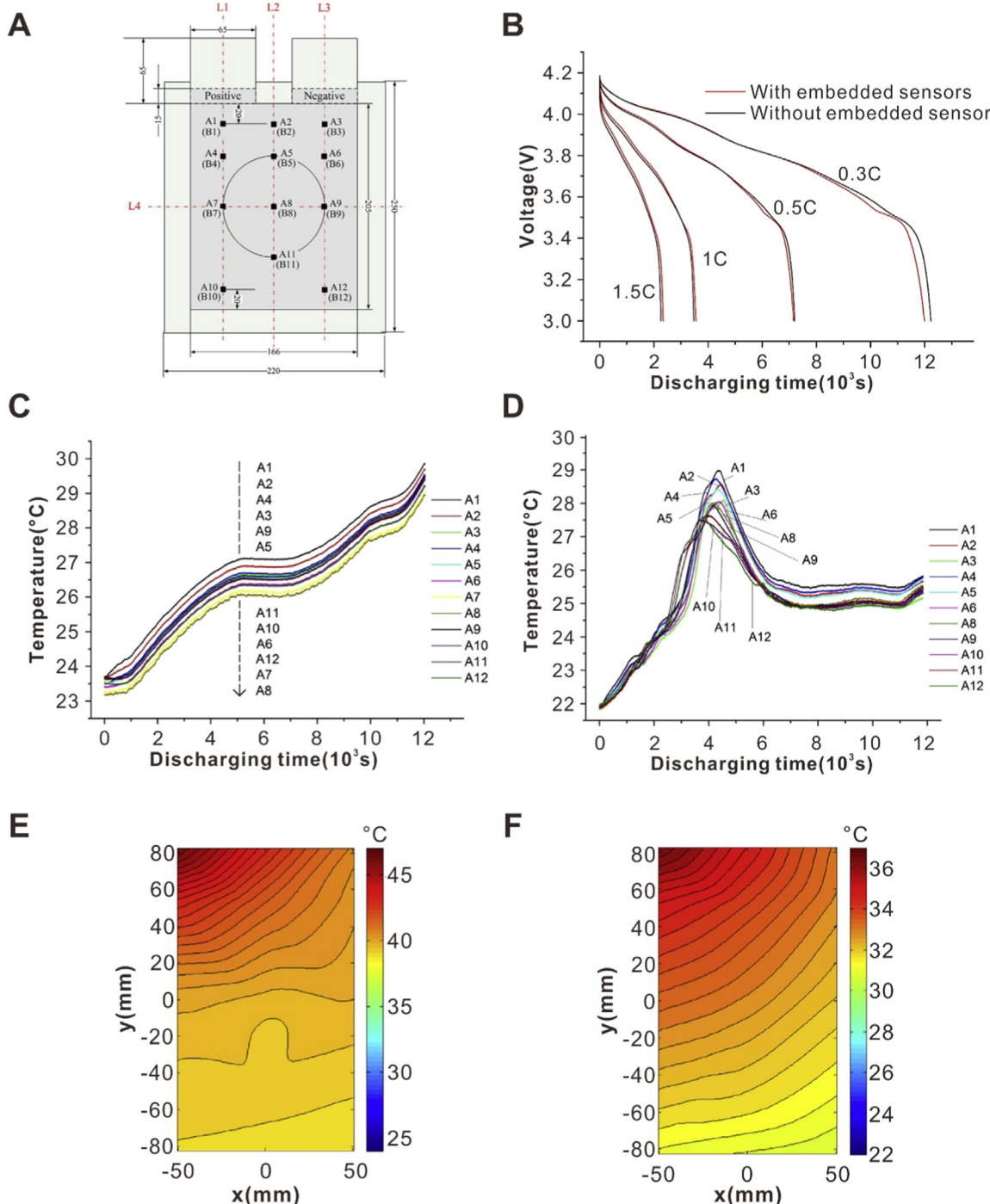


**Fig. 8.** (A) Schematic of the locations of the embedded thermocouples. A1~A12: inside; B1-B12: surface. (B) The discharge curves of tested batteries with and without embedded sensors at different discharge rates. (C, D) Temperature curves at the 12 tested points at 0.3C discharge rate under (C) adiabatic condition and (D) natural convection condition. (E, F) Spatial distribution of internal temperature at maximum temperature rise at 1C discharge rate under (E) adiabatic condition and (E) natural convection. Reproduced with permission from [115]. Copyright: 2013, Elsevier.

which generates heat and promotes the elevation of temperature inside the batteries. Stage III starts with the melting of polyethylene (PE) separators at 130–140  $^{\circ}$ C, which leads to the micro internal shorting (stage IV) and the continuing rise of temperature. At this temperature condition, the decomposition of anodes continues and consumes the active materials in anodes. As the temperature reaches above 240  $^{\circ}$ C, the decomposition of cathode materials, electrolytes and binders occurs. Such series of chemical reactions produce large amounts of heat that rapidly increases the temperature to 800  $^{\circ}$ C or higher and leads to fire with the existence of oxygen released by the cathode reactions.

These reactions also generate other gaseous products, which increase the internal pressure of batteries, and may even result in unexpected explosion at high temperature.

In this section, we overviewed the temperature effects to LIBs, including both the low temperature effects and the high temperature effects. Those effects not only lead to the degradation of performance in LIBs, but also may result in lithium plating and thermal runaway. These effects indicate that the performance of LIBs is closely dependent on temperature. Monitoring of the temperature inside LIBs is therefore a critical process in minimizing temperature effects. In the following

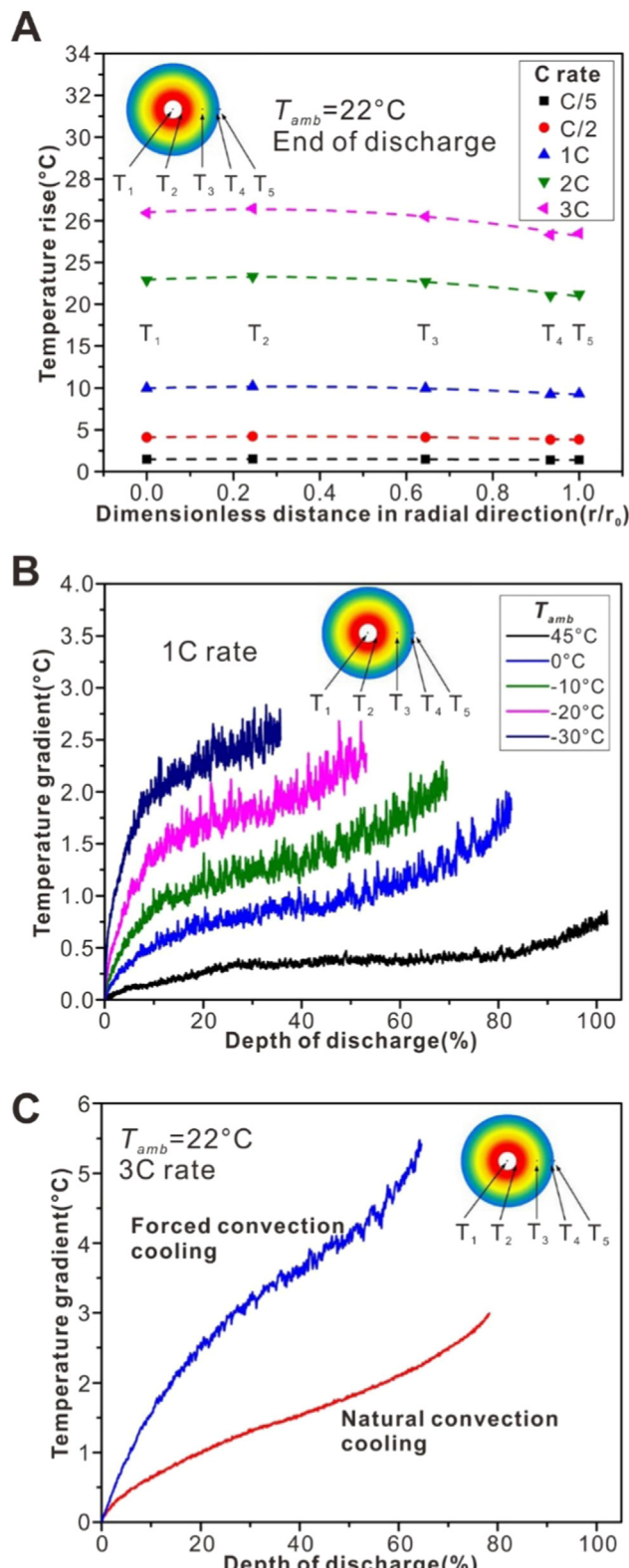


**Fig. 9.** (A) Radical distribution of temperature rise at the end of discharge at different discharge rate. (B) Variation of temperature gradient at 1C discharge rate under different ambient temperature conditions. The temperature gradient was defined as  $T_2-T_5$ . (C) Comparison of the temperature gradient variation at 3C discharge rate between the forced convection cooling and the natural convection cooling. Reproduced with permission from [116]. Copyright: 2014, ECS.

sections we will review the efforts in monitoring temperature inside the LIBs.

### 3. Approaches for internal temperature monitoring of LIBs

The distribution of temperature at the surface of batteries is easy to acquire with common temperature measurement approaches, such as the use of thermocouples and thermal imaging systems [111]. It is, however, challenging to use these approaches in monitoring the internal temperature of LIBs. The self-production of heat during operation can elevate the temperature of LIBs from inside. The transfer of heat from interior to exterior of batteries is difficult due to the multilayered structures and low coefficients of thermal conductivity of battery components [112–114]. The spatial distribution of internal temperature is also uneven [83].

In consideration of the sealed nature and the electrochemical reactions of LIBs during operation, researchers tried to explore different approaches in monitoring the internal temperature of LIBs. As illustrated in Fig. 7, these approaches can be classified into two main categories: contact measurement and contactless measurement. In contact measurement, temperature sensors such as thermocouples and Fiber Bragg Grating (FBG) sensors are inserted into LIBs to measure the temperature directly. In contrast, in the contactless measurement, the internal temperature was obtained indirectly without intruding into the batteries. Modeling simulation and electrochemical impedance are two major contactless approaches. In the modeling simulation, electrochemical and thermal models were established to simulate the operation of LIBs in different situations and theoretically estimate the internal temperature. Predicting the internal temperature using electrochemical impedance is another contactless method. The electrochemical impedance of LIBs is a temperature-dependent parameter. By establishing calibration curves of the relationships between impedance and temperature, the internal temperature of LIBs can be estimated. In this section, we will discuss the present approaches for both contact measurement and contactless measurement of internal temperature of the LIBs.

#### 3.1. Contact measurement

Implanting thermal sensors into LIBs is the most direct way to measure the internal temperature. Li et al. [115] monitored the spatial and temporal variations of internal temperature of a laminated battery with pre-embedded thermocouples. The battery was operated at different discharge rates and ambient conditions during the temperature measurement. Fig. 8A shows the locations of thermocouples within the tested batteries. The overlapping of discharge curves of batteries with and without embedded thermocouples indicated that the impact of the inserted sensors on the performance of batteries was negligible (Fig. 8B). When the battery discharged at the rate of 0.3C, the average temporal internal temperature under adiabatic condition gradually rose from 23.5 °C to 29 °C with the increase of discharging time (Fig. 8C). Differently, under natural convection condition, the temperature reached a peak value of 29 °C and decreased to a plateau of 25.5 °C during discharging (Fig. 8D). This difference indicates that natural convection can help establish an equilibrium between the generation and dissipation of heat within the batteries. The internal temperature at each location was generally higher than that at the surface, in which the maximum difference was 1.1 °C at location 2 (Fig. 8A) when the battery discharged at 1.5C rate under natural convection. Fig. 8E and F show the spatial distribution of internal temperature under adiabatic condition and natural convection condition, respectively. Temperature gradients appeared from the top left to the bottom right spatially, in which the hot zones located closely to the anode tabs. This result was corresponding to the higher current densities near electrode tabs and the more heat generation at anode tabs than that at cathode tabs. This work provides a good example of monitoring the internal temperature of LIBs

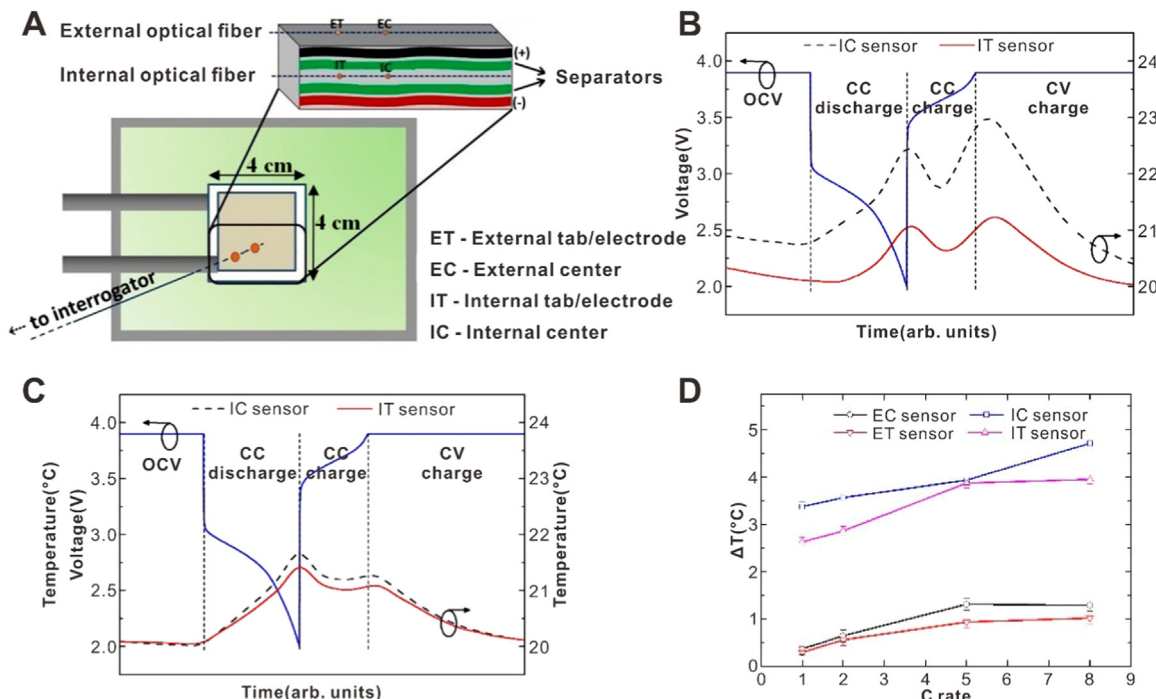


**Fig. 10.** (A) Schematic of the locations of FBG sensors. (B) Variation of internal temperature under corresponding operation process of the tested battery. (C) Variation of external temperature under corresponding operation process of the tested battery. (D) Maximum temperature difference measured at corresponding C rates. Reproduced with permission from [117]. Copyright: 2016, MDPI AG.

with embedded thermocouples. It shows the inhomogeneous distribution of temperature inside working LIBs, which also demonstrates the necessity of multi-point measurement.

Zhang et al. [116] also measured the internal temperature of LIBs with embedded micro-thermocouples. Rather than using the laminated pouch battery, the battery they used for testing was a commercial 18650 cylindrical cell. The locations of thermocouples were along the radius of battery as shown in Fig. 9. The temperatures at these locations were examined under different discharge rates, both at ambient temperatures and cooling conditions. The result in Fig. 9A indicates that higher discharge rate caused more generation of heat, and resulted in higher increase of temperature at each location and larger temperature gradient along the radius of the battery. Fig. 9B shows that the temperature gradient under lower ambient temperature increased faster than that under higher ambient temperature. Such difference was due to the more efficient dissipation of heat at outer layers under low ambient temperature conditions than under the high ambient temperature conditions. The forced convection cooling also led to larger temperature gradient than cooling by natural convection (Fig. 9C).

In addition to thermocouples, other micro thermal sensors that can be integrated into LIBs are also capable of detecting the internal temperature of LIBs. Novais et al. [117] measured the temperature variation of an assembled pouch battery under various operating conditions with FBG sensors. The measurement locations included two internal points and the corresponding external points (Fig. 10A). Fig. 10B and C show that the temperature fluctuated up and down with the progress of operation. The temperature inside the battery varied, both temporally and spatially, much more than that at the surface. The maximum temperature difference ( $\Delta T$ ) increased with charge/discharge rate, in which the internal  $\Delta T$  was as large as  $4.7^{\circ}\text{C}$  at 8C rate (Fig. 10D). This work demonstrated that the variation of temperature was correlated to the state of applied voltage, with peaks appearing at the end of charge and discharge. Such temperature change was attributed to the fact that over charge and discharge, the ion distribution becomes inhomogeneous, which leads to heat generation.

Implanting thermal sensors into LIBs is a feasible approach to

monitor the internal temperature experimentally, as demonstrated in the above researches. It is, however, not suitable for practical applications. Integration of thermal sensors is destructive to the structure of LIBs. Moreover, insulation layers are often needed to cover on the probes of thermal sensors [115,116,118] to minimize the disturbance of components within the batteries during measurement. These covering layers affect the accuracy of measurement due to the thermal resistance from these insulation layers.

### 3.2. Contactless measurement

In order to avoid the damage to the structure of li-ion batteries, contactless and nondestructive measurement is developed. Modeling simulation and electrochemical impedance-based process are two typical approaches for contactless measurement of internal temperature of the LIBs.

#### 3.2.1. Modeling simulation

Recent researches on modeling simulation for estimating the internal temperature of LIBs mainly include two types. One is the thermal model that simply concerns the thermal aspects inside batteries, while another one is the thermal-electric model that considers both the thermal and electric aspects. Forgez et al. [119] reported a representative thermal model for cylindrical LIBs that can estimate the internal temperature from surface temperature. To make it compatible with the low computational resources of micro-controllers used in battery management systems (BMSs), Forgez et al. established their thermal model without coupling it with electrochemical models. Fig. 11A shows the completed thermal model of the tested battery based on the analysis of heat generation and heat transfer. The detailed parameters in the model, however, are too complex to be determined. By assuming that the internal temperature of the battery was uniformly distributed, authors proposed a simplified model as presented in Fig. 11B. With this simplified model, the internal temperature of cylindrical LIBs can be estimated as

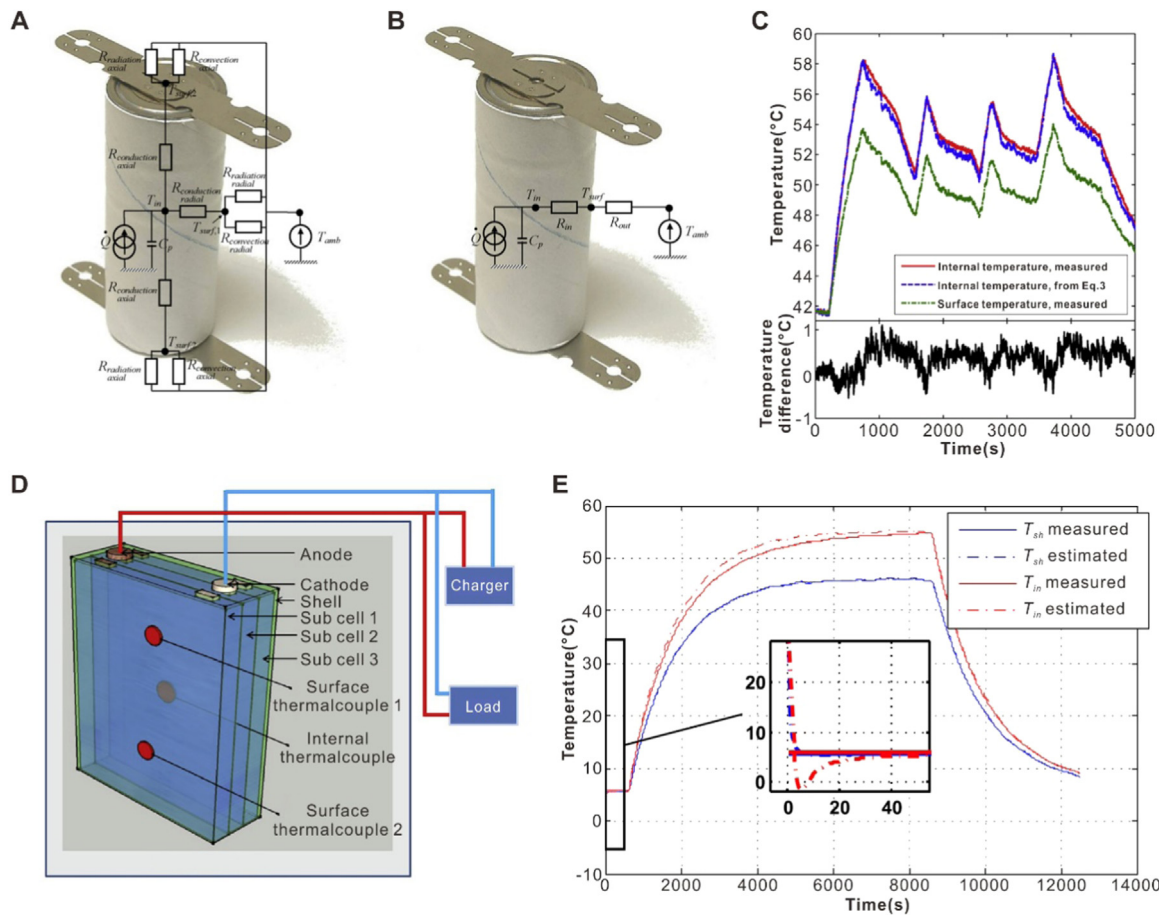


**Fig. 11.** Illustration of the (A) completed and (B) simplified thermal models. (C) Temperature variations measured by experiment and estimated from Eq. (3), and temperature difference between experimental and estimated results. (A-C) Reproduced with permission from [119]. Copyright: 2010, Elsevier. (D) Illustration of the battery test system. (E) Comparison of the measured and estimated temperature variation in one period of current pulse.  $T_{sh}$  is the surface temperature and  $T_{in}$  is the internal temperature. (D-E) Reproduced with permission from [120]. Copyright: 2016, Elsevier.

$$T_{in} = T_{surf} \left( 1 + \frac{R_{in}}{R_{out}} \right) - T_{amb} \frac{R_{in}}{R_{out}} \quad (3)$$

In Eq. (3),  $T_{in}$ ,  $T_{surf}$  and  $T_{amb}$  represent internal temperature, surface temperature, and ambient temperature, respectively.  $R_{in}$  and  $R_{out}$  are the thermal resistance inside and outside the batteries. To verify the accuracy of this equation, the estimated results of internal temperature were compared with the experimental results, which were obtained with inserted thermocouples. The overlapping of the estimated curve and measured curve in Fig. 11C proved the feasibility of this model, and the difference between the estimated temperature and the measured temperature was within 1.5 °C.

Kim et al. [121] proposed another thermal model for cylindrical batteries that can estimate the distribution of internal temperature along radius of the batteries. Specifically, the authors pointed out that the information of the cooling condition to the batteries was also essential to the accurate estimation of internal temperature even though the surface temperature was known. With this thermal model, both the internal core temperature and convection coefficient of the tested battery were identified. The previous reports assumed that the internal temperature was uniform under certain thermal conditions. This work extended the modeling methods to accurately estimate the distribution of internal temperature of LIBs under unknown cooling conditions.

Although the proposed thermal models can be used to predict the internal temperature to some extent, they do not take into account of the electric actions within the operating LIBs. The thermal process and electric process inside a working LIB are often coupled together. For example, the heat generation inside the LIBs is correlated with the

internal resistance. The increase of the internal temperature can lead to the drop of the battery resistance, and in turn affect the heat generation. The change of resistance will also affect the battery power. Therefore, several researches paid attention to the establishment of thermal-electric models that consider the interactions between thermal and electrical processes. Zhang et al. [120] reported a representative thermal-electric model that offered a comprehensive description of the behavior of LIBs. In that work, they first set up the electric submodel from the battery electric circuit model and also the thermal submodel from analysis of heat generation and transfer, respectively. To simplify the simulation, the heat generation and distribution of temperature within the battery were assumed to be uniform. Based on the shared parameters, these two submodels were coupled together and the thermal-electric model was established. With this model, the authors evaluated the accuracy of the estimation of both internal and surface temperatures by using the test system shown in Fig. 11D. Fig. 11E shows the estimated results and measured results during a period of 30A current pulse. Both the curves of surface temperature and internal temperature exhibited good overlapping between estimated and measured results. A maximum temperature difference of 8 °C existed between the internal center and external surface of the battery.

The modeling simulation extends the approaches to estimate the temperature inside LIBs with improving computational technologies, but it still has unavoidable deficiency. The complex conditions of LIBs during operation produce various intricate factors, which are difficult to determine experimentally.

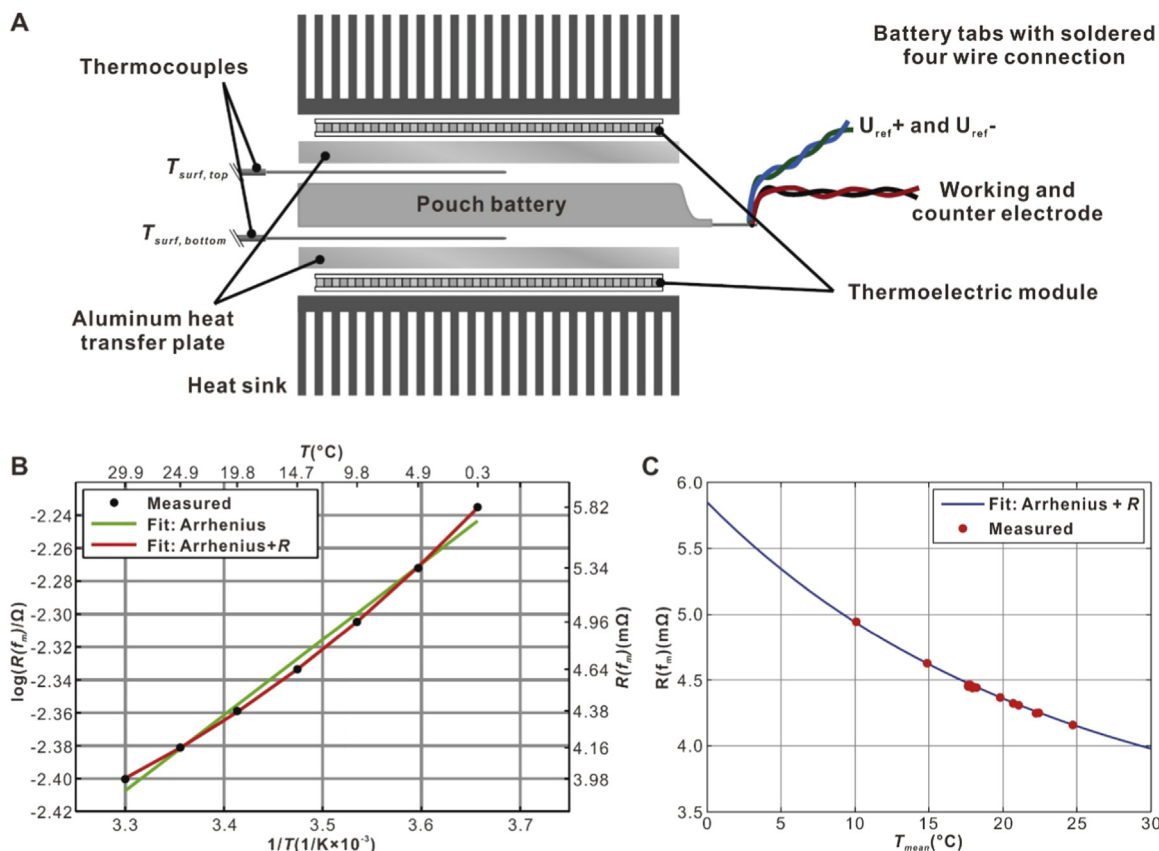


**Fig. 12.** (A) Schematic of the experimental setup. (B) Correlation between the real part of impedance and internal temperature under spatially homogeneous temperature conditions. (C) Correlation between the real part of impedance and internal temperature under spatially inhomogeneous temperature conditions. The temperature conditions were controlled by applying different top and bottom heating parameters. The impedance was determined at a frequency of 10.3 kHz and a constant SOC of 50%. Reproduced with permission from [122]. Copyright: 2013, Elsevier.

### 3.2.2. Electrochemical impedance-based measurement

Although it is challenging to directly measure the internal temperature of LIBs, it is relatively straightforward to measure the electrochemical impedance of LIBs by using common electrochemical workstations. Such impedance measurement provides an opportunity to indirectly obtain the information of temperature within LIBs. A calibration curve of impedance-temperature can be experimentally measured, and the internal temperature can be derived from the calibration curve. The determination of electrochemical impedance is based on the Electrochemical Impedance Spectroscopy (EIS). EIS is a diagnostic method, in which a frequency-varying sinusoidal current is applied to the electrochemical system. The response of impedance variation to the frequency is then measured. The correlation of impedance, SOC and internal temperature of the tested LIBs can be obtained using EIS.

The electrochemical impedance in LIBs is described in the form of complex number, which contains parameters such as real part, imaginary part and phase. Researchers often use one of these parameters to predict the internal temperature of LIBs. Schmidt et al. [122] estimated the internal temperature of a pouch battery by measuring the change of real part of electrochemical impedance. In addition to the temperature, the electrochemical impedance is also relevant to SOC in certain range of frequency. The frequency of sinusoidal current thus should be controlled to avoid the disturbance of SOC. Schmidt and co-workers used a thermal chamber to heat the battery to an equilibrium state at different temperature conditions, and assumed the distribution of temperature in the entire battery to be uniform (Fig. 12A). Fig. 12B and C recorded the values of the real part of impedance under spatially homogeneous and inhomogeneous temperature conditions. The temperature points were set as the mean values of  $T_{surf,top}$  and  $T_{surf,bottom}$ . The calibration curves were established by fitting the acquired data points. The fitted

calibration curves were corresponding to a corrected Arrhenius equation, in which the corrected error was related to the electric conductivity of the metallic collector. They reported that the precision of this proposed method reached  $\pm 0.17K$  with known SOC status and  $\pm 2.5K$  with unknown SOC status under isothermal conditions.

Phase is another parameter of the electrochemical impedance that is relevant to the internal temperature and SOC of LIBs. Upon the change of temperature at certain frequency, the phase angle will shift in a predictable direction. By utilizing this correlation, Srinivasan et al. [123] quantized the relationship between phase shift and internal temperature of three types of LIBs. Similar to Schmidt's work, the temperature of batteries was also controlled at the uniform state by a thermal chamber. The frequency of EIS was controlled in the range of 40–100 Hz. This range allowed the phase shift of the three batteries to be only dependent on the temperature. The phase shift upon temperature change displayed an Arrhenius behavior from  $-20$ – $66$  °C, which showed a similar trend as the real part did in Schmidt's work. The authors also pointed out that the temperature-dependent variation of impedance was relevant to the ionic conduction in the SEI layers. The behavior of SEI layers also plays a significant role in analyzing the aging of LIBs. Therefore, these studies on predicting temperature from impedance measurement not only provide alternative approaches to the estimation of internal temperature, but also offer feedback to the condition of SEI layers that may enable proper management of LIBs.

The studies discussed above demonstrated the capability of estimating internal temperature using the parameters of electrochemical impedance. All the temperature states in experiments, however, are set to be the mean temperature. The distribution of temperature in LIBs in real applications is mostly uneven. Large difference exists between the maximum temperature and the mean temperature. To overcome this

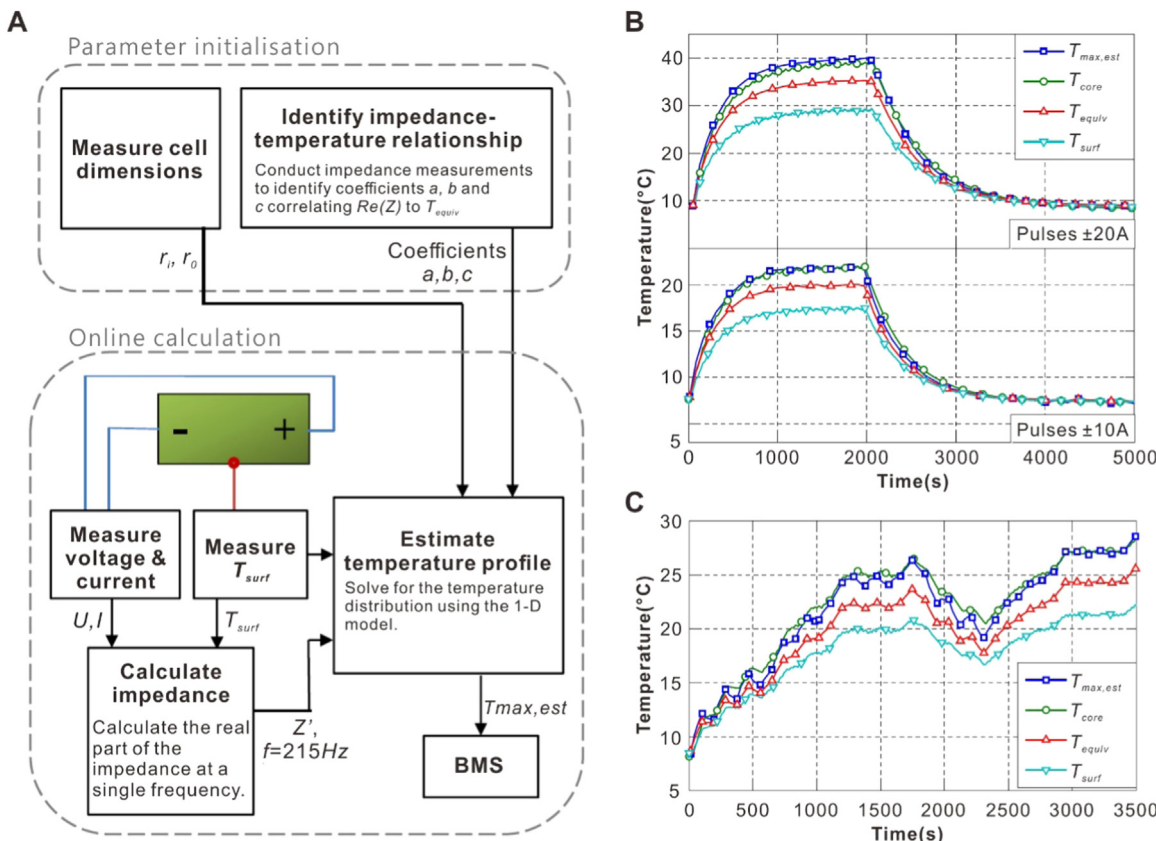


**Fig. 13.** (A) Modeling process of real-time internal temperature estimation for LIBs. (B, C) Temperature validation with (B) current pulse method and (C) HEV drive cycle method. Reproduced with permission from [124]. Copyright: 2014, Elsevier.

problem, Richardson et al. [124] introduced a model that combined the impedance and surface temperature of LIBs together. The proposed thermal-impedance model was able to predict the temperature gradient along the radius of cylindrical batteries. Different from the principles applied in traditional models, this method treated the cylindrical battery using Calculus. In this model, the battery was split into infinitesimal concentric annuli that were electrically connected, and each of the unit was temperature-dependent in radius. Detailed description about the model can be referred to Richardson's work [124]. Fig. 13A shows the flow of the modeling process. As the only required inputs were impedance and surface temperature, and no complex computed programming was needed, the model was simple enough to implement in BMSs. They also validated the model experimentally with a thermocouple-implanted cylindrical 26,650 battery by two heating approaches: current pulse and a 3500 s HEV drive cycle current. Fig. 13B and C show the comparison between the modeling results and the experimental results. The maximum temperature ( $T_{max, est}$ ) represented the modeling results with impedance measured at 215 Hz, while the equivalent uniform temperature ( $T_{equiv}$ ) was derived from the measurement of corresponding impedance. The core temperature ( $T_{core}$ ) and surface temperature ( $T_{surf}$ ) were obtained by using thermocouples.  $T_{max, est}$  and  $T_{core}$  show a good consistency with each other, but  $T_{equiv}$  shows an obvious gap from them. The mean absolute error between  $T_{max, est}$  and  $T_{core}$  during the cycle test was 0.6 °C, while it increased to 2.6 °C if the distribution of internal temperature was considered uniform and derived from impedance alone.

#### 4. Conclusions

Thermal challenges exist in the applications of LIBs due to the temperature-dependent performance. The optimal operating temperature range of LIBs is generally limited to 15–35 °C. Both low

temperature and high temperature out of this scope will affect the performance and may cause irreversible change to the LIBs. At low temperatures, the degradation of performance is mainly caused by the reduction of ionic conductivity and the increase of charge-transfer resistance. Lithium plating is a specific effect that occurs on the surface of graphite and other carbon-based anodes, which leads to the loss of capacity at low temperatures. High temperature conditions accelerate the thermal aging and may shorten the lifetime of LIBs. Heat generation within the batteries is another considerable factor at high temperatures. With the stimulation of elevated temperature, the exothermic reactions are triggered and generate more heat, leading to the further increase of temperature. Such uncontrolled heat generation will result in thermal runaway.

In this review, we also overviewed recent studies on the monitoring of the internal temperature of LIBs. Present approaches include contact measurement and contactless measurement. Contact measurement mainly includes the implantation of thermal sensors into LIBs, and contactless measurement includes modeling simulation and impedance-based estimation. Each of them, whether contact measurement or contactless measurement, has its own advantages and disadvantages. For the contact measurement by using micro-thermal sensors, it is feasible to achieve the spatial distribution of temperature by arranging multiple detectors at various locations in the batteries. The shortcoming of contact measurement is that implanting temperature probes will certainly lead to the destruction to the batteries, which will be challenging to implement such approach in practical use. The delay of thermal transfer from hot spots to sensors and the insulation layer on the probes can also induce the measurement errors. These disadvantages limit the application of the contact measurement approaches. Modeling simulation and impedance-based estimation solve this problem by indirectly obtaining the internal temperature without intruding into the batteries. At present the temperature in most models

are assumed to be uniform, while in reality the distribution of temperature in batteries is inhomogeneous.

To control the operating temperature of LIBs and ensure the performance and safety, various battery thermal management systems (BTMSs) are designed for the thermal management of LIBs. For the batteries working under high temperature conditions, the current cooling strategies are mainly based on air cooling [125,126], liquid cooling [127,128] and phase change material (PCM) cooling [129,130]. Air cooling and liquid cooling, obviously, are to utilize the convection of working fluid to cool the batteries. Generally, the heat transfer coefficient of liquid is higher than that of air, making it more efficient as the working medium and attracting more attentions of researchers. The PCM cooling is to use the phase change materials, of which the phase change point is within the desirable temperature scope of the LIBs, as the heat transfer mediums. Below the phase change point, the heat is conducted to PCMs and accumulated. When the temperature reaches the point, the mediums melt or vaporize and take away the heat from batteries. Compared to the various cooling systems, the heating strategies for LIBs need to be explored further. Several researches proposed heating methods through modeling simulation and experimental practice, such as internal heating resistance [131] and external preheating system [132,133]. So far these progresses of BTMSs are preliminarily able to counter the temperature effects to LIBs, but still have a long way to go. The comprehensive study on the mechanism of thermal effects and temperature monitoring inside LIBs may provide ideas theoretically and help to build up BTMSs systematically.

## Acknowledgements

P. Tao, T. Deng and W. Shang are grateful to the financial support from National Key R&D Program of China, Ministry of Science and Technology of the People's Republic of China, China (Grant No. 2017YFB0406100), and National Natural Science Foundation of China, China (Grant No. 51521004, 51420105009), and the 111 Project, Ministry of Education of the People's Republic of China, China (Grant No: B16032).

## References

- [1] R. Cecchini, G. Pelosi, IEEE Antennas Propag. Mag. 34 (1992) 30–37.
- [2] P. Cotti, Phys. B 204 (1995) 367–369.
- [3] M. Piccolino, Trends Neurosci. 23 (2000) 147–151.
- [4] V.S. Bagotsky, J. Solid State Electrochem. 15 (2011) 1559–1562.
- [5] A.C. Marschilok, Y.J. Kim, K.J. Takeuchi, E.S. Takeuchi, J. Electrochem. Soc. 159 (2012) A1690–A1695.
- [6] K. Zhang, X. Han, Z. Hu, X. Zhang, Z. Tao, J. Chen, Chem. Soc. Rev. 46 (2015) 2376–2404.
- [7] X.P. Gao, H.X. Yang, Energy Environ. Sci. 3 (2010) 174–189.
- [8] F. Rahmawati, L. Yulianti, I.S. Alaih, F.R. Putri, J. Environ. Chem. Eng. 5 (2017) 2251–2258.
- [9] M. Selvam, S.R. Srithar, K. Saminathan, V. Rajendran, Ionics 21 (2015) 791–799.
- [10] S.H. Joo, S.M. Shin, D.J. Shin, J.P. Wang, Proc. Inst. Mech. Eng. Part B 229 (2015) 212–220.
- [11] X. Song, S. Hu, D. Chen, B. Zhu, J. Ind. Ecol. 21 (2017) 57–69.
- [12] K. Yoo, S.M. Shin, D.H. Yang, J.S. Sohn, Miner. Eng. 23 (2010) 219–224.
- [13] B. Liao, Y.Q. Lei, L.X. Chen, G.L. Lu, H.G. Pan, Q.D. Wang, J. Power Sources 129 (2004) 358–367.
- [14] T. Sakai, H. Ishikawa, K. Oguro, C. Iwakura, H. Yoneyama, J. Electrochem. Soc. 134 (1987) 558–562.
- [15] S.R. Ovshinsky, M.A. Fetcenko, J. Ross, Science 260 (1993) 176–181.
- [16] L. Ji, Z. Lin, M. Alcoutabi, X. Zhang, Energy Environ. Sci. 4 (2011) 2682–2699.
- [17] E.J. Yoo, J. Kim, E. Hosono, H. Zhou, T. Kudo, I. Honma, Nano Lett. 8 (2008) 2277–2282.
- [18] J.M. Tarascon, M. Armand, Nature 414 (2001) 359–367.
- [19] N. Yabuuchi, K. Kubota, M. Dahbi, S. Komaba, Chem. Rev. 114 (2014) 11636–11682.
- [20] M.D. Slater, D. Kim, E. Lee, C.S. Johnson, Adv. Funct. Mater. 23 (2013) 947–958.
- [21] H. Pan, Y.S. Hu, L. Chen, Energy Environ. Sci. 6 (2013) 2338–2360.
- [22] R. Marom, S.F. Amalraj, N. Leifer, D. Jacob, D. Aurbach, J. Mater. Chem. 21 (2011) 9938–9954.
- [23] L.X. Yuan, Z.H. Wang, W.X. Zhang, X.L. Hu, J.T. Chen, Y.H. Huang, J.B. Goodenough, Energy Environ. Sci. 4 (2011) 269–284.
- [24] Y. Wang, G. Cao, Adv. Mater. 20 (2008) 2251–2269.
- [25] L. Lu, X. Han, J. Li, J. Hua, M. Ouyang, J. Power Sources 226 (2013) 272–288.
- [26] G.E. Blomgren, J. Electrochem. Soc. 164 (2017) A5019–A5025.
- [27] J.B. Goodenough, Acc. Chem. Res. 46 (2013) 1053.
- [28] <https://pushevs.com/2017/03/15/technology-regulation-motivation/>.
- [29] D. Linden, T.B. Reddy, Handbook of Batteries, fourth ed., McGraw Hill, New York, 2011.
- [30] H. Meng, X. Pang, Z. Zhen, J. Power Sources 237 (2013) 229–242.
- [31] R. Santhanam, B. Rambabu, J. Power Sources 195 (2010) 5442–5451.
- [32] T.C. Wanger, Conserv. Lett. 4 (2011) 202–206.
- [33] Y. Wang, H. Li, P. He, E. Hosono, H. Zhou, Nanoscale 2 (2010) 1294–1305.
- [34] X.K. Feng, B.L. Wang, A.S. Chen, Q.X. Yang, Chin. J. Power Sources 26 (2002) 63–65.
- [35] B. Scrosati, J. Hassoun, Y.K. Sun, Energy Environ. Sci. 4 (2011) 3287–3295.
- [36] C. Liu, F. Li, L.P. Ma, H.M. Cheng, Adv. Mater. 22 (2010) E28–E62.
- [37] D.R. Pendergast, E.P. Demauro, M. Fletcher, E. Stimson, J.C. Mollendorf, J. Power Sources 196 (2011) 793–800.
- [38] M.C. Smart, B.V. Ratnakumar, L.D. Whitcanack, F.J. Puglia, S. Santee, R. Gitzendanner, Int. J. Energy Res. 34 (2010) 116–132.
- [39] T. Minato, T. Abe, Prog. Surf. Sci. 92 (2017) 240–280.
- [40] B. Li, D. Xia, Adv. Mater. 29 (2017) 1701054.
- [41] J.B. Goodenough, Y. Kim, Chem. Mater. 22 (2010) 587–603.
- [42] Y. Ji, Y. Zhang, C.Y. Wang, J. Electrochem. Soc. 160 (2013) A636–A649.
- [43] A. Pesaran, S. Santhanagopalan, G.H. Kim, Addressing the Impact of Temperature Extremes on Large Format Li-Ion Batteries for Vehicle Applications, Presented at: Proceedings of the 30th International Battery Seminar, Ft. Lauderdale, Florida, 2013.
- [44] Z. Yang, Q.H.S. Li, J. Mao, J. Alloy. Compd. 753 (2018) 192–202.
- [45] D.P. Finegan, E. Darcy, M. Keyser, B. Tjaden, T.M.M. Heenan, R. Jervis, J.J. Bailey, N.T. Vo, O.V. Magdysyuk, M. Drakopoulos, M.D. Michiel, A. Rack, G. Hinds, D.J.L. Brett, P.R. Shearing, Adv. Sci. 5 (2018) 1870003.
- [46] F. He, X. Li, G. Zhang, G. Zhong, J. He, Int. J. Energy Res. 42 (2018) 3279–3288.
- [47] D. Ren, K. Smith, D. Guo, X. Han, X. Feng, L. Lu, M. Ouyang, J. Li, J. Electrochem. Soc. 165 (2018) A2167–A2178.
- [48] J. Jaguemont, L. Boulon, Y. Dubé, Appl. Energy 164 (2016) 99–114.
- [49] S. Panchal, J. McGrory, J. Kong, R. Fraser, M. Fowler, I. Dincer, M. Agelin-Chaab, Int. J. Energy Res. 41 (2017) 2565–2575.
- [50] T.M. Bandhauer, S. Garimella, T.F. Fuller, J. Electrochem. Soc. 158 (2011) (R1-R25).
- [51] R. Bugga, M. Smart, J. Whitacre, W. West, Lithium Ion Batteries for Space Applications, in: Proceedings of the IEEE Aerospace Conference, Big Sky, MT, USA, pp. 1–7, 2007.
- [52] H.C. Shiao, D. Chua, H.P. Lin, S. Slane, M. Salomon, J. Power Sources 87 (2000) 167–173.
- [53] S.S. Zhang, K. Xu, T.R. Jow, Electrochim. Acta 48 (2002) 241–246.
- [54] K. Yang, J.J. An, S. Chen, Sci. China Chem. 53 (2010) 1177–1182.
- [55] Q.F. Yuan, F. Zhao, W. Wang, Y. Zhao, Z. Liang, D. Yan, Electrochim. Acta 178 (2015) 682–688.
- [56] P. Ramadas, B. Haran, R. White, B.N. Popov, J. Power Sources 112 (2002) 614–620.
- [57] J.R. Belt, C.D. Ho, T.J. Miller, M.A. Habib, T.Q. Duong, J. Power Sources 142 (2005) 354–360.
- [58] Y. Zhang, C.Y. Wang, X. Tang, J. Power Sources 196 (2011) 1513–1520.
- [59] J. Shim, R. Kostecki, T. Richardson, X. Song, K.A. Striebel, J. Power Sources 112 (2002) 222–230.
- [60] G. Ning, B. Haran, B.N. Popov, J. Power Sources 117 (2003) 160–169.
- [61] J.R. Belt, C.D. Ho, C.G. Motloch, T.J. Miller, T.Q. Duong, J. Power Sources 123 (2003) 241–246.
- [62] R. Spotzni, J. Franklin, J. Power Sources 113 (2003) 81–100.
- [63] Q. Wang, P. Ping, X. Zhao, G. Chu, J. Sun, C. Chen, J. Power Sources 208 (2012) 210–224.
- [64] K.J. Laidler, J. Chem. Educ. 61 (1984) 494–498.
- [65] S.S. Zhang, K. Xu, T.R. Jow, J. Solid State Electrochem. 7 (2003) 147–151.
- [66] S.C. Nagpure, R. Dinwiddie, S. Babu, G. Rizzoni, B. Bhushan, T. Frech, J. Power Sources 195 (2010) 872–876.
- [67] T.R. Jow, S.A. Delp, J.L. Allen, J.P. Jones, M.C. Smart, J. Electrochem. Soc. 165 (2018) A361–A367.
- [68] G. Nagasubramanian, J. Appl. Electrochem. 31 (2001) 99–104.
- [69] X. Zhang, W. Zhang, H. Li, M. Zhang, Trans. Electr. Electron. Mater. 18 (2017) 136–140.
- [70] A.M. Aris, B. Shabani, Energy Procedia 110 (2017) 128–135.
- [71] H. Wang, H. Zhang, Y. Cheng, K. Feng, X. Li, H. Zhang, Electrochim. Acta 278 (2018) 279–289.
- [72] Q. Li, S. Jiao, L. Luo, M.S. Ding, J. Zheng, S.S. Cartmell, C.M. Wang, K. Xu, J.G. Zhang, W. Xu, ACS Appl. Mater. Interfaces 9 (2017) 18826–18835.
- [73] S.C. Kinoshita, M. Kotato, Y. Sakata, M. Ue, Y. Watanabe, H. Morimoto, S.I. Tobishima, J. Power Sources 183 (2008) 755–760.
- [74] B. Yang, H. Zhang, L. Yu, W.Z. Fan, D. Huang, Electrochim. Acta 221 (2016) 107–114.
- [75] Q. Li, S. Jiao, L. Luo, M.S. Ding, J. Zheng, S.S. Cartmell, C.M. Wang, K. Xu, J.G. Zhang, W. Xu, ACS Appl. Mater. Interfaces 9 (2017) 18826–18835.
- [76] F. Gao, Z. Tang, Electrochim. Acta 53 (2008) 5071–5075.
- [77] S.S. Zhang, K. Xu, T.R. Jow, J. Power Sources 115 (2003) 137–140.
- [78] X.H. Rui, Y. Jin, X.Y. Feng, L.C. Zhang, C.H. Chen, J. Power Sources 196 (2011) 2109–2114.
- [79] M. Petzl, M.A. Danzer, J. Power Sources 254 (2014) 80–87.
- [80] V. Zinth, C.V. Lüders, M. Hofmann, J. Hattendorff, I. Buchberger, S. Erhard, J. Rebelo-Kornmeier, A. Jossen, R. Gilles, J. Power Sources 271 (2014) 152–159.

- [81] M. Petzl, M. Kasper, M.A. Danzer, *J. Power Sources* 275 (2015) 799–807.
- [82] N. Gunawardhana, N. Dimov, M. Sasidharan, G.J. Park, H. Nakamura, M. Yoshio, *Electrochim. Commun.* 13 (2011) 1116–1118.
- [83] H. Liu, Z. Wei, W. He, J. Zhao, *Energy Convers. Manag.* 150 (2017) 304–330.
- [84] M. Xiao, S.Y. Choe, *J. Power Sources* 241 (2013) 46–55.
- [85] X. Zhang, *Electrochim. Acta* 56 (2011) 1246–1255.
- [86] D. Bernardi, E. Pawlikowski, J. Newman, *J. Electrochem. Soc.* 132 (1985) 5–12.
- [87] Y. Hui, J. Prakash, *J. Electrochem. Soc.* 151 (2004) A1222–A1229.
- [88] W. Lu, J. Prakash, *J. Electrochem. Soc.* 150 (2003) A262–A266.
- [89] M. Balasundaram, V. Ramar, C. Yap, L. Li, A.A.O. Tay, P. Bayala, *J. Power Sources* 328 (2016) 413–421.
- [90] A. Nazari, S. Farhad, *Appl. Therm. Eng.* 125 (2017) 1501–1517.
- [91] Y. Lai, S. Du, L. Ai, L. Ai, Y. Cheng, Y. Tang, M. Jia, *Int. J. Hydrog. Energy* 40 (2015) 13039–13049.
- [92] S. Du, Y. Lai, L. Ai, L. Ai, Y. Cheng, Y. Tang, M. Jia, *Appl. Therm. Eng.* 121 (2017) 501–510.
- [93] A. Nyman, T.G. Zavalis, R. Elger, M. Behm, G. Lindbergh, *J. Electrochem. Soc.* 157 (2010) A1236–A1246.
- [94] X.G. Yang, G. Zhang, C.Y. Wang, *J. Power Sources* 328 (2016) 203–211.
- [95] B. Yan, C. Lim, L. Yin, L. Zhu, *Electrochim. Acta* 100 (2013) 171–179.
- [96] J. Esmaeilii, H. Jannesari, *Energy Convers. Manag.* 139 (2017) 194–205.
- [97] T.G. Zavalis, M. Klett, M.H. Kjell, M. Behm, R.W. Lindström, G. Lindbergh, *Electrochim. Acta* 110 (2013) 335–348.
- [98] M. Ecker, N. Nieto, S. Käbitz, J. Schmalstieg, H. Blanke, A. Warnecke, D.U. Sauer, *J. Power Sources* 248 (2014) 839–851.
- [99] Y. Liu, K. Xie, Y. Pan, Y. Li, H. Wang, W. Lu, C. Zheng, *Ionics* 24 (2017) 723–734.
- [100] E. Markevich, E. Pollak, G. Salitra, D. Aurbach, *J. Power Sources* 174 (2007) 1263–1269.
- [101] H. Gabrisch, Y. Ozawa, R. Yazami, *Electrochim. Acta* 52 (2006) 1499–1506.
- [102] L. Bodenes, R. Naturel, H. Martinez, R. Dedryvère, M. Menetrier, L. Croguennec, J.P. Péres, C. Tessier, F. Fischer, *J. Power Sources* 236 (2013) 265–275.
- [103] T. Waldmann, M. Wilka, M. Kasper, M. Fleischhammer, M. Wohlfahrt-Mehrens, *J. Power Sources* 262 (2014) 129–135.
- [104] P. Handel, G. Fauler, K. Kapper, M. Schmuck, C. Stangl, R. Fischer, F. Uhlig, S. Koller, *J. Power Sources* 267 (2014) 255–259.
- [105] F. Leng, C.M. Tan, M. Pecht, *Sci. Rep.* 5 (2015) 12967.
- [106] T. Ohsaki, T. Kishi, T. Kuboki, N. Takami, N. Shimura, Y. Sato, M. Sekino, A. Satoh, *J. Power Sources* 146 (2005) 97–100.
- [107] <[https://money.cnn.com/2006/08/24/technology/apple\\_recall/index.htm](https://money.cnn.com/2006/08/24/technology/apple_recall/index.htm)>.
- [108] <<https://www.cpsc.gov/cpscpub/prerel/prhtml06/06270.html>>.
- [109] D.P. Finegan, M. Scheel, J.B. Robinson, B. Tjaden, I. Hunt, T.J. Mason, J. Millilchamp, M. Di Michiel, G.J. Offer, G. Hinds, *Nat. Commun.* 6 (2015) 6924.
- [110] X. Feng, M. Fang, X. He, M. Ouyang, L. Lu, H. Wang, M. Zhang, *J. Power Sources* 255 (2014) 294–301.
- [111] J.B. Robinson, P.R. Shearing, D.J. Brett, *J. Imaging* 2 (2016) 2.
- [112] V. Vishwakarma, A. Jain, *J. Power Sources* 272 (2014) 378–385.
- [113] Y. Yang, X. Huang, Z. Cao, G. Chen, *Nano Energy* 22 (2016) 301–309.
- [114] H. Maleki, S.A. Hallaj, J.R. Selman, R.B. Dinwiddie, H. Wang, *J. Electrochem. Soc.* 146 (1999) 947–954.
- [115] Z. Li, J. Zhang, B. Wu, J. Huang, Z. Nie, Y. Sun, F. An, N. Wu, *J. Power Sources* 241 (2013) 536–553.
- [116] G. Zhang, L. Cao, S. Ge, C.-Y. Wang, C.E. Shaffer, C.D. Rahn, *J. Electrochem. Soc.* 161 (2014) A1499–A1507.
- [117] S. Novais, M. Nascimento, L. Grande, M.F. Domingues, P. Antunes, N. Alberto, C. Leitão, R. Oliveira, S. Koch, G.T. Kim, *Sensors* 16 (2016) 1394.
- [118] S. Drake, M. Martin, D. Wetz, J. Ostank, S. Miller, J. Heinzel, A. Jain, *J. Power Sources* 285 (2015) 266–273.
- [119] C. Forgez, D.V. Do, G. Friedrich, M. Morcrette, C. Delacourt, *J. Power Sources* 195 (2010) 2961–2968.
- [120] C. Zhang, K. Li, J. Deng, *J. Power Sources* 302 (2016) 146–154.
- [121] Y. Kim, S. Mohan, J.B. Siegel, A.G. Stefanopoulou, Y. Ding, *IEEE Trans. Control Syst. Technol.* 22 (2014) 2277–2286.
- [122] J.P. Schmidt, S. Arnold, A. Loges, D. Werner, T. Wetzel, E. Ivers-Tiffée, *J. Power Sources* 243 (2013) 110–117.
- [123] R. Srinivasan, B.G. Carkhuff, M.H. Butler, A.C. Baisden, *Electrochim. Acta* 56 (2011) 6198–6204.
- [124] R.R. Richardson, P.T. Ireland, D.A. Howey, *J. Power Sources* 265 (2014) 254–261.
- [125] S.K. Mohammadian, S.M. Rassoulinejad-Mousavi, Y. Zhang, *J. Power Sources* 296 (2015) 305–313.
- [126] S.C. Yong, D.M. Kang, *J. Power Sources* 270 (2014) 273–280.
- [127] D. Chen, J. Jiang, G.H. Kim, C. Yang, A. Pesaran, *Appl. Therm. Eng.* 94 (2016) 846–854.
- [128] T. Wei, K. Somasundaram, E. Birgersson, A.S. Mujumdar, C. Yap, *Int. J. Therm. Sci.* 94 (2015) 259–269.
- [129] C.V. Hémery, F. Pra, J.F. Robin, P. Marty, *J. Power Sources* 270 (2014) 349–358.
- [130] G. Jiang, J. Huang, M. Liu, M. Cao, *Appl. Therm. Eng.* 120 (2017) 1–9.
- [131] X.G. Yang, T. Liu, C.Y. Wang, *J. Power Sources* 342 (2017) 598–604.
- [132] Y. Ji, C.Y. Wang, *Electrochim. Acta* 107 (2013) 664–674.
- [133] T. Zhu, H. Min, Y. Yu, Z. Zhao, T. Xu, Y. Chen, X. Li, C. Zhang, *Energies* 10 (2017) 243.